

An Improved Technique for the Photometry and Astrometry of Faint Companions

DANIEL BURKE

School of Physics, National University of Ireland, Galway, Ireland; daniel.burke@nuigalway.ie

SZYMON GLADYSZ

European Organisation for Astronomical Research in the Southern Hemisphere; sgladysz@eso.org

LEWIS ROBERTS

Jet Propulsion Laboratory, California Institute of Technology; lewis.c.roberts@jpl.nasa.gov

NICHOLAS DEVANEY

School of Physics, National University of Ireland, Galway, Ireland; nicholas.devaney@nuigalway.ie

AND

CHRIS DAINTY

School of Physics, National University of Ireland, Galway, Ireland; c.dainty@nuigalway.ie

Received 2009 May 19; accepted 2009 June 5; published 2009 June 29

ABSTRACT. We propose a new approach to differential astrometry and photometry of faint companions in adaptive optics images. It is based on a prewhitening matched filter, also referred to in the literature as the Hotelling observer. We focus on cases where the signal of the companion is located within the bright halo of the parent star. Using real adaptive optics data from the 3 m Shane telescope at the Lick Observatory, we compare the performance of the Hotelling algorithm with other estimation algorithms currently used for the same problem. The real single-star data are used to generate artificial binary objects with a range of magnitude ratios. In most cases, the Hotelling observer gives significantly lower astrometric and photometric errors. In the case of high Strehl ratio (SR) data ($SR \approx 0.5$), the differential photometry of a binary star with a $\Delta m = 4.5$ and a separation of $0.6''$ is better than 0.1 mag; a factor of 2 lower than the other algorithms considered.

1. INTRODUCTION

Differential astrometry and photometry of faint companions in adaptive optics (AO) observations is an important new problem in astronomy (Roberts et al. 2005, 2007). Methods are currently being developed for application to Extremely Large Telescope (ELT) images of exoplanets (Kasper et al. 2008). For exoplanets, differential photometry can be used to derive the planetary mass assuming one of the theoretical models for either reflected or internal light (Baraffe et al. 2003). Hence, an estimate of the planet's mass could in principle be derived from a single image. The importance of accurate binary star photometry lies in determining one of the most basic properties of a star: its mass. When the mass of a survey of stars is estimated accurately, this information can serve as a test of stellar formation and evolution models (Turner et al. 2008).

We propose a new likelihood-maximization method based on using the Hotelling observer (Barrett et al. 1995) to extract astrometry and photometry of faint companions in AO-corrected images. The Hotelling observer is an algorithm derived from

statistical decision theory. When used to detect features, the algorithm/observer applies one or more linear operations to the data and the results of these operations are used to make a decision regarding the nature of the recorded feature, e.g., whether it represents a signal or noise. Furthermore, a modified version of the algorithm can be used to estimate features of objects already classified as real. In this article, we discuss the estimation accuracy of the Hotelling observer and not its reliability as a detection scheme; for the latter, see Caucci et al. (2007).

The accuracy of the Hotelling approach is compared to other commonly used algorithms using test data. The chosen algorithms are StarFinder (Diolaiti et al. 2000) and Fitstars (ten Brummelaar et al. 2000). In § 2 we review these and other algorithms which have been applied to the tasks of extracting astrometry and photometry from AO images of binary stars. The Hotelling observer for computing astrometry and photometry is derived in § 3. In § 4 a description of the observations and data reduction is presented, followed in § 5 with a comparison of the astrometric and photometric accuracy of the three algorithms.

The paper concludes in § 6 with a discussion of the performance of the algorithm and some suggestions for future study.

2. STANDARD APPROACHES TO AO PHOTOMETRY AND ASTROMETRY

There are three main approaches to deriving photometry from stellar images; aperture photometry, PSF fitting, and deconvolution. The latter two techniques also extract relative astrometry.

Digital aperture photometry can be carried out using the APPHOT package (Davis 1989) within the IRAF environment (Shames & Tody 1986). The technique uses pixel integration over a user-defined aperture in the image. No knowledge of the point-spread function (PSF) is needed as no PSF-fitting techniques are used. This method works best on uncrowded star fields where there is no overlap of light from nearby stars.

It is often the case that images of close binary stars do have overlapping profiles, in which case aperture photometry is not suitable for extracting differential photometry. Stetson (1987) was one of the first to propose using PSF fitting for this problem. In the PSF-fitting approach, an analytic or empirical PSF is used together with a fitting algorithm to match scaled-and-shifted copies of this PSF to the data. The photometric accuracy of this method depends mostly on the accuracy of the PSF estimate. This estimate can be obtained by describing the PSF analytically or numerically. The most commonly used analytical PSFs are Gaussian, Lorentzian, or Franz functions (Devaney 1992). This analytical approach works best when the images are critically sampled (Nyquist), or undersampled (Stetson et al. 1990). In the second approach, the empirical PSF is extracted directly from the observations. If there is a bright isolated star in an image, then a subarray containing this isolated star will provide an empirical model of the PSF. This is best implemented on oversampled data (Stetson 1992).

A combination of these methods has been implemented in the DAOPHOT II software package (Stetson 1992). An analytical function is first fitted to the data for several bright isolated stars, and scaled copies of this profile are then subtracted from the original data. The subarrays containing the residuals are extracted and averaged together. The estimated PSF is then a combination of the analytical PSF and an interpolation on the residuals. This method works best when the analytic function accounts for over 90% of the profile shape within the “true” PSF.

A more recent implementation of the PSF-fitting concept is the StarFinder package (Diolaiti et al. 2000). The code, which has a graphical user interface, was developed for the specific purpose of measuring relative photometry and astrometry in AO-corrected stellar fields. The algorithm operates in two stages: initial PSF estimation and iterative PSF fitting. In the first stage, bright isolated stars in the image are identified and background-subtracted. The resulting subimages are then registered with subpixel accuracy, normalized, and median-

combined to produce the first PSF estimate. A synthetic field consisting of delta functions convolved with the PSF estimate is then subtracted from the data. In the second stage, the residual image is searched via cross-correlation with the PSF template for additional sources. Images of the detected secondary sources are then fitted with the PSF estimate. The result of this is relative astrometry and photometry, as well as an updated estimate of the PSF. The process is iterated until no sources can be reliably found in the residuals. The deconvolution approach is based on the image formation equation

$$i(x, y) = o(x, y) * p(x, y) + n(x, y), \quad (1)$$

where x and y are focal-plane coordinates, i is the image, o is the exact representation of the object in the focal plane, $p(x, y)$ is the system PSF, which is assumed to be isoplanatic, i.e., it does not vary over the field, $*$ denotes convolution and n comprises all the noise terms. Equation (1) can be written in the Fourier domain

$$I = O \times P + N, \quad (2)$$

where capital letters denote the Fourier transformation of the function represented by the corresponding lower case letter, i.e., I is the Fourier transform of i . This form suggests a simple deconvolution method—having a PSF, an estimate of the object could be obtained by inverting equation (2). Unfortunately this inversion leads to amplification of noise, which is always present in the observations. This effect can be partly alleviated by using a Wiener filter in the inversion of equation (2) (Press et al. 1986).

In AO-corrected astronomical observations the PSF is never known exactly. A further complication is that the AO PSF can have a complex asymmetric form. In this case both the object and the PSF have to be extracted from the data. This is referred to as blind deconvolution (Stockham et al. 1975). Ayers & Dainty (1988) proposed an iterative algorithm to solve for two positive functions, o and p , which provide the best solution to equation (1).

The algorithm works in the following manner: firstly, a non-negative-valued initial estimate of o is input to the iterative algorithm; this function is then Fourier transformed to yield \tilde{O} ; the tilde denotes an estimate of the function \tilde{O} is then inverted to form an inverse filter and multiplied by I (eq. [2]) to form P_0 . This estimated Fourier spectrum is then inverse transformed to give p_0 , the first estimate of the PSF. A nonnegativity constraint is then applied to p_0 and it is then Fourier transformed to give \tilde{P}_0 . This function is then inverted and multiplied by I to give the next estimate \tilde{O}_1 . The iterative loop is completed by inverse Fourier transforming \tilde{O}_1 to give o_1 and applying a nonnegativity constraint to yield \tilde{o}_1 . The loop is repeated until two positive estimates of o and p , which satisfy the required convolution \tilde{i} , are found.

Lane (1992) showed that this algorithm does not converge in a stable way. For example, an extra iteration of the Ayers-Dainty algorithm may result in new estimates of o and p that are worse, both in terms of their error metric and visually, than the previous estimates. Lane proposed to perform deconvolution by minimizing an error metric function E which imposes constraints in both Fourier and image spaces. The minimization technique he used was a conjugate gradient approach (Fletcher 1987). In practice the algorithm produces a series of estimates of o and p which have a decreasing value of the function E with each iteration. The algorithm converges when a minimum of E has been found.

This iterative blind deconvolution (IBD) framework was further refined by Jefferies & Christou (1993). Their error metric function contained four contributions to the metric. As before, an error metric in the image and Fourier spaces was included, as well as an error metric for a band-limit constraint on the PSF and an error metric for the Fourier modulus. The conjugate gradient routine from Press et al. (1986) was used to minimize the combined error metric. They applied their IBD algorithm to a wide range of astronomical images and detected a third component in the binary system 85 Pegasi.

Fitstars (ten Brummelaar et al. 2000) is an iterative blind deconvolution algorithm optimized for binary stars. It extracts differential photometry and astrometry of the two stellar components, as well as the PSF corresponding to the observations. The object is assumed to consist of two δ functions. If the intensity of the i th star is A_i and its position is (x_i, y_i) , we can write the object as

$$o(x, y) = \sum_{i=1}^2 A_i \delta(x - x_i, y - y_i). \quad (3)$$

Using an initial guess for the PSF, this equation can be solved in a least-squares sense for the positions and magnitudes of the stars in the field. The sample PSF can be taken from an image of a single star, or the result from a previous operation of Fitstars. Even a relatively poor initial guess of the PSF will converge and produce similar results. The PSF changes substantially between observations of different targets due to changes in seeing and variations in AO performance on different targets. In order to compensate for this, a new model of the PSF is extracted from the data using the fitted estimates of the position and magnitude differences. An estimate of the PSF based on the star k is

$$p_k(x, y) = i(x, y) - \sum_{j \neq k} A_j [\delta(x - x_j, y - y_j) * p_{k-1}(x, y)]. \quad (4)$$

An estimate of the PSF can be extracted for each star in the field, and a new PSF is formed by use of a weighted average over the PSF estimates (ten Brummelaar et al. 1996)

$$p_{\text{new}}(x, y) = \frac{1}{\sum_j A_j} \times \sum_j A_j p_k(x, y). \quad (5)$$

This p_{new} is a new PSF model and the process can be repeated until the results converge. Fitstars has been used with adaptive optics data sets from several telescopes with results which compared well to other methods (Horch et al. 2001; Pluzhnik 2005).

3. THE HOTELLING OBSERVER

The Hotelling observer is sometimes referred to as a prewhitening matched filter (Barrett et al. 2006a). In the process of prewhitening, the data are divided by the data covariance matrix with the aim of producing spatially stationary, uncorrelated noise. In this article we use an image of a reference star—a calibration PSF—to obtain an estimate of the data covariance matrix. This PSF is used to subtract the signal of the bright star from the image (PSF subtraction), flatten the residuals (prewhitening), and estimate the companion's signal via matched filtering. Data prewhitening and matched filtering is not unique to the Hotelling observer; the generalized Wiener-Helstrom filter (Helstrom 1968; Barrett et al. 1995; Barrett et al. 2006a) also uses second order statistics of the object, and forms its output by a linear operation on prewhitened data. However, the Wiener-Helstrom filter is biased toward the a priori mean and this is not the case for the Hotelling observer.

The task we are concerned with is the estimation of the location and intensity of a faint companion in an AO-corrected image. It is, however, convenient to introduce the nomenclature corresponding to faint companion detection. In this case, for a given data set g there are two hypotheses to be considered: H_1 refers to the case when a companion is present in the data and H_0 refers to the hypothesis that it is absent. One of our assumptions is that the data were already preprocessed, so that they are flat-fielded and background-subtracted. Also, if the observations consist of multiple images, we assume that these frames have been recentered and co-added. The algorithm/observer is now supplied with a preprocessed long-exposure image.

Let \bar{g}_0 denote the mean image when a companion is absent; the overbar refers to the mean of the data averaged over the measurement noise. When a companion is present, at the position r_{pl} , the mean image is written as $\bar{g}_{1,r_{pl}}$. The true signal of the companion is then given by

$$s_{r_{pl}} = \bar{g}_{1,r_{pl}} - \bar{g}_0. \quad (6)$$

In real life situations, astronomical images are contaminated by several types of noise, such as cosmic ray hits, bad pixels on the detector, readout noise from the detector, and noise due to the stochastic nature of photon detection. Bad pixels and cosmic ray hits can usually be compensated for by applying a median

filter to the data (Artigau et al. 2008). The noisy images are modeled under the two hypotheses as

$$H_0: g = \bar{g}_0 + n, \quad H_{1,r_{pl}}: g = \underbrace{\bar{g}_0 + s_{r_{pl}}}_{\bar{g}_{1,r_{pl}}} + n. \quad (7)$$

The noise n is composed of Gaussian noise from the detector readout and Poisson noise arising from the detection of the incident radiation. We do not consider spatially correlated static (Gladysz & Christou 2008) or pinned (Bloemhof et al. 2001) speckle noise. This is because it is very difficult in practice to obtain information on the statistics of the correlated speckle noise. Theoretically there is nothing preventing the use of a full covariance matrix in equations (9) and (10). Nevertheless we will show that very good results can be obtained with our algorithm assuming uncorrelated noise, i.e., a diagonal covariance matrix. A possible approach to include speckle noise in the covariance matrix is to use data from image-plane wavefront sensors (Vasisht et al. 2006).

In the following we assume that the data with dimensions of $n \times n$ have been rearranged into column vectors of size $M \times 1$, where $M = n \times n$. This rearrangement makes it possible to use normal matrix operations on the data. The noisy images can now be expressed as

$$\begin{aligned} \bar{g}_0 &= \underbrace{A_* h(r_*)}_{\text{star image}} + \underbrace{b}_{\text{background}}, \\ \bar{g}_{1,r_{pl}} &= \underbrace{A_* h(r_*)}_{\text{star image}} + \underbrace{A_{pl} h(r_{pl})}_{\text{companion image}} + \underbrace{b}_{\text{background}}, \end{aligned} \quad (8)$$

where A_* is the intensity of the bright star located at position r_* , A_{pl} is the intensity of the companion located at r_{pl} , $h(r)$ is the PSF located at r , and b is the background intensity.

While the intensity in AO-corrected short exposures has a modified Rician distribution (Cagigal & Canales 1998; Aime & Soummer 2004), the sum of these intensities, over many exposures, can be approximated by a Gaussian distribution by the central limit theorem. Therefore we expect the intensity statistics in an ensemble of long-exposure images to obey Gaussian statistics. Under the Gaussian assumption, the densities $pr(g|H_0)$ and $pr(g|H_{1,r_{pl}})$ can then be expressed as (Helstrom 1968; Caucci et al. 2007)

$$\begin{aligned} pr(g|H_0) &= \left[\frac{1}{(2\pi)^M \det(K_g)} \right]^{1/2} \\ &\times \exp \left[-\frac{1}{2} (g - \bar{g}_0)^T K_g^{-1} (g - \bar{g}_0) \right], \end{aligned} \quad (9)$$

$$\begin{aligned} pr(g|H_{1,r_{pl}}) &= \left[\frac{1}{(2\pi)^M \det(K_g)} \right]^{1/2} \\ &\times \exp \left[-\frac{1}{2} (g - \bar{g}_0 - s_{r_{pl}})^T \right. \\ &\left. \times K_g^{-1} (g - \bar{g}_0 - s_{r_{pl}}) \right]. \end{aligned} \quad (10)$$

Here \det denotes the determinant of a given matrix; 0000^T denotes transpose; $pr(g|H)$ is the conditional probability density function of the data under the hypothesis H , either H_0 or $H_{1,r_{pl}}$; and K_g is the covariance matrix of the data, of size $M \times M$.

With the assumption of uncorrelated noise, the data covariance matrix, K_g , is diagonal, with elements given by

$$[K_g]_{m,m'} = [A_* h_m(r_*) + b_m + \sigma_m^2] \delta_{m,m'}, \quad (11)$$

where $\delta_{m,m'}$ is the Kronecker delta function, σ^2 is the variance of the detector readout noise, and m represents the pixel index.

For the tasks of differential astrometry and photometry of faint companions, the optimal discriminant function, referred to as the ideal observer, is the likelihood ratio (Barrett & Myres 2004)

$$\Lambda(g|r_{pl}) = \frac{pr(g|H_{1,r_{pl}})}{pr(g|H_0)}. \quad (12)$$

If the companion location r_{pl} is unknown, the ideal observer can be applied at a set of test locations R and is referred to as the ideal scanning observer (Caucci et al. 2007). This observer is at a maximum at the true companion location, $r_{pl} \in R$. This means that the algorithm can be used to estimate the differential astrometry of a companion. The ideal scanning observer takes on the form

$$\Lambda(g) = \max_{r_{pl} \in R} \Lambda(g|r_{pl}) = \max_{r_{pl} \in R} \frac{pr(g|H_{1,r_{pl}})}{pr(g|H_0)}. \quad (13)$$

The estimation of r_{pl} is then computed as

$$\tilde{r}_{pl} = \arg \max_{r_{pl} \in R} \Lambda(g|r_{pl}). \quad (14)$$

Under the assumption of Gaussian noise (eq. [9] and [10]), taking the logarithm of $\Lambda(g)$ we obtain the log-likelihood ratio, $\lambda(g) = \ln[\Lambda(g)]$, given by

$$\begin{aligned}
\lambda(g) &= \max_{r_{pl} \in R} \left[\frac{1}{2} (g - \bar{g}_0)^T K_g^{-1} (g - \bar{g}_0) \right. \\
&\quad \left. - \frac{1}{2} (g - \bar{g}_0 - s_{r_{pl}})^T K_g^{-1} (g - \bar{g}_0 - s_{r_{pl}}) \right] \\
&= \max_{r_{pl} \in R} -\frac{1}{2} \left[-g^T K_g^{-1} (g - \bar{g}_0) + \bar{g}_0^T K_g^{-1} (g - \bar{g}_0) \right. \\
&\quad \left. + g^T K_g^{-1} (g - \bar{g}_0 - s_{r_{pl}}) - \bar{g}_0^T K_g^{-1} (g - \bar{g}_0 - s_{r_{pl}}) \right. \\
&\quad \left. - s_{r_{pl}}^T K_g^{-1} (g - \bar{g}_0 - s_{r_{pl}}) \right]. \quad (15)
\end{aligned}$$

If K_g^{-1} is diagonal, as we assumed earlier (eq. [11]), then

$$\begin{aligned}
\lambda(g) &= \max_{r_{pl} \in R} -\frac{1}{2} \left[-g^T K_g^{-1} s_{r_{pl}} + \bar{g}_0^T K_g^{-1} s_{r_{pl}} \right. \\
&\quad \left. - s_{r_{pl}}^T K_g^{-1} g + s_{r_{pl}}^T K_g^{-1} \bar{g}_0 + s_{r_{pl}}^T K_g^{-1} s_{r_{pl}} \right] \\
&= \max_{r_{pl} \in R} -\frac{1}{2} \left[2s_{r_{pl}}^T K_g^{-1} (\bar{g}_0 - g) + s_{r_{pl}}^T K_g^{-1} s_{r_{pl}} \right] \\
&= \max_{r_{pl} \in R} \left[s_{r_{pl}}^T K_g^{-1} (g - \bar{g}_0 - \frac{1}{2} s_{r_{pl}}) \right]. \quad (16)
\end{aligned}$$

The quantity that appears in square brackets in equation (16) is linear, or more properly affine, in g . The log-likelihood ratio, $\lambda(g)$, is therefore the ideal linear observer. Barrett et al. (2006b) show that the Hotelling observer, $t_{\text{Hot}}(g)$, is equal to the log-likelihood ratio if the data are normally distributed with equal covariances under both hypotheses, i.e., $K_{g|H_1} = K_{g|H_0}$. In equation (16), the signal of the bright parent star and half of the predicted companion signal is removed from the data. The subtraction of half of the predicted companion signal does not affect the location of the maximum of $\lambda(g)$. The result is pre-whitened, i.e., divided by the data covariance matrix K_g . The output of this operation is then processed with a matched filter using the expected companion signal located at the expected companion position, r_{pl} . Following on from equation (16): recalling from equation (11) the expression for $K_g = A_* h_m(r_*) + b_m + \sigma_m^2$ and $s_{r_{pl}} = \bar{g}_{1,r_{pl}} - \bar{g}_0 = A_{pl} h_m(r_{pl})$, we can write an expression for the scanning Hotelling observer, $t_{\text{Hot}}(g)$, in the form

$$\begin{aligned}
t_{\text{Hot}}(g) &= \max_{r_{pl} \in R} \sum_{m=1}^M \frac{A_{pl} h_m(r_{pl})}{A_* h_m(r_*) + b_m + \sigma_m^2} \\
&\quad \times \left[g_m - \bar{g}_{0,m} - \frac{1}{2} A_{pl} h_m(r_{pl}) \right]. \quad (17)
\end{aligned}$$

The estimation of the companion location, r_{pl} , is then computed as

$$\tilde{r}_{pl} = \arg \max_{r_{pl} \in R} [t_{\text{Hot}}(g)]. \quad (18)$$

In the following, equation (18) is referred to as the Spatial Scanning Hotelling Estimator (SSHE). The operator of the algorithm computes a set of scalars on the data g . These scalars are functions of the unknown position of the companion r_{pl} . The maximum of this set of scalars is taken as the value of the Hotelling observer, $t_{\text{Hot}}(g)$. In this derivation of the SSHE, it was assumed that the intensity of the companion A_{pl} was known. In general, for faint companions this will not be the case. However, the Hotelling method can be generalized to estimate both the companion's position, r_{pl} , and intensity, A_{pl} , at the same time. The maximum of equation (17) is now dependent upon the Cartesian product of the two unknown parameters: r_{pl} and A_{pl} . However, this is a computationally intensive approach.

The approach we take in this article relies on the fact that for every estimate of the location of the companion, there exists an estimate of the intensity of the companion that maximizes the Hotelling test statistic for that location. Recalling the log-likelihood ratio, equation (16), the estimate of the companion's intensity, A_{pl} , for a defined set of test intensities A becomes

$$\tilde{A}_{pl} = \arg \max_{A_{pl} \in A} \left[s_{r_{pl}}^T K_g^{-1} (g - \bar{g}_0) - \frac{1}{2} s_{r_{pl}}^T K_g^{-1} s_{r_{pl}} \right]. \quad (19)$$

Equation (19) assumes that r_{pl} is known. The log-likelihood ratio is maximized by taking the partial derivative with respect to A_{pl} and setting it equal to zero

$$\frac{\partial t_{\text{Hot}}(g)}{\partial A_{pl}} = h(r_{pl})^T K_g^{-1} (g - \bar{g}_0) - A_{pl} h(r_{pl})^T K_g^{-1} h_m(r_{pl}) = 0, \quad (20)$$

where we made use of the fact that $s_{r_{pl}} = A_{pl} h(r_{pl})$. This leads to the following estimator for A_{pl} :

$$\tilde{A}_{pl} = \frac{h(r_{pl})^T K_g^{-1} (g - \bar{g}_0)}{h(r_{pl})^T K_g^{-1} h(r_{pl})}. \quad (21)$$

Recalling the structure of the data covariance matrix K_g , we get

$$\tilde{A}_{pl} = \sum_{m=1}^M \frac{(h_m(r_{pl}) / (A_* h_m(r_*) + b_m + \sigma_m^2)) [g_m - \bar{g}_{0,m}]}{h_m(r_{pl})^2 / (A_* h_m(r_*) + b_m + \sigma_m^2)}, \quad (22)$$

where m is the pixel index of the image. We refer to equation (22) as the Optimal Hotelling Estimator (OHE). The estimation of the companion location is computed using the SSHE while substituting the OHE's estimation of A_{pl} into the SSHE for each test location. The result is astrometry and photometry of an observed companion.

The mathematical form of the OHE can be compared to that of the iterative blind deconvolution equation (Barnaby et al. 2000). This algorithm uses a conjugate gradient minimization to minimize the error metric

$$E_f = \sum_k \left[g_k - (\tilde{o}_k * \tilde{p}_k) \right]^2, \quad (23)$$

where k is the pixel index, o represents the object (in the focal plane), p is an estimate of the PSF, and g is the observed data. The object, o , can be divided into two signals (equation [3]): the bright star, and the companion signal

$$E_f = \sum_k \left[g_k - A_*(\delta(x - x_*, y - y_*)) * \tilde{p}_k \right. \\ \left. - A_{pl}(\delta(x - x_{pl}, y - y_{pl})) * \tilde{p}_k \right]^2. \quad (24)$$

As above, instead of using a gradient minimization, an expression for this minimum can be found by taking the partial derivative of E_f with respect to A_{pl} and setting it equal to zero:

$$\frac{\partial E_f}{\partial A_{pl}} = 2 \sum_k \left[g_k - A_*(\delta(x - x_*, y - y_*)) * \tilde{p}_k \right. \\ \left. - A_{pl}(\delta(x - x_{pl}, y - y_{pl})) * \tilde{p}_k \right] \\ \Rightarrow \sum_k \left[g_k - A_*(\delta(x - x_*, y - y_*)) * \tilde{p}_k \right. \\ \left. - A_{pl}(\delta(x - x_{pl}, y - y_{pl})) * \tilde{p}_k \right] = 0. \quad (25)$$

This leads to the estimation of A_{pl} :

$$\tilde{A}_{pl} = \sum_k \frac{[g_k - A_*(\delta(x - x_*, y - y_*)) * \tilde{p}_k]}{[\delta(x - x_{pl}, y - y_{pl})) * \tilde{p}_k]}. \quad (26)$$

It is instructive to compare equations (22) and (26). The difference is that in equation (22), the PSF-subtracted data are pre-

whitened, then cross-correlated with a matched filter. The same operations are applied to the PSF. The importance of prewhitening will be shown in § 4.

4. OBSERVATIONS AND DATA REDUCTION

In order to compare the photometric and astrometric accuracy of the proposed approach with PSF-fitting and IBD, we used data obtained with the Lick Observatory AO system on the 3 m Shane telescope (Bauman et al. 1999). Closed loop images of bright, single stars were obtained using the high-speed subarray mode with a size of 64×64 pixels of the 256×256 pixel IRCAL camera (Fitzgerald & Graham 2006). This corresponds to a field size of $4.864'' \times 4.864''$. The subarray measurements were captured with typical exposure times of 22 ms. Each data set comprised 10,000 images. All data were obtained in the K band ($2.2 \mu\text{m}$) where the diffraction limit is 151 mas, so that the data were effectively Nyquist sampled. The individual short exposures were registered with subpixel accuracy to produce shift-and-add (SAA) images. The average SR of these SAA images was around 40%. For the details of the observations and data reduction, see Gladysz et al. (2006).

In order to establish the effect of the prewhitening operation on the data, the peak-signal-to-noise ratio (PSNR) will be compared for the PSF-subtracted data and the prewhitened PSF-subtracted data (see Fig. 1). The signal-to-noise ratio (S/N) is defined as the ratio of the mean to the standard deviation of the measured data (Roggemann 1996). The binary system HD170648 ($m_k = 7.21$, $\Delta m_k = 3.07$, separation $\theta = 0.69''$, spectral type A2) was observed along with a properly matched calibration PSF (HD 173869: $m_V = 7.9$, $m_K = 7.53$, spectral type A0) (Gladysz et al. 2008). The covariance matrix of the data (eq. [11]) was computed as follows: the intensity of the central star, A_* , was estimated using the calibration PSF in a

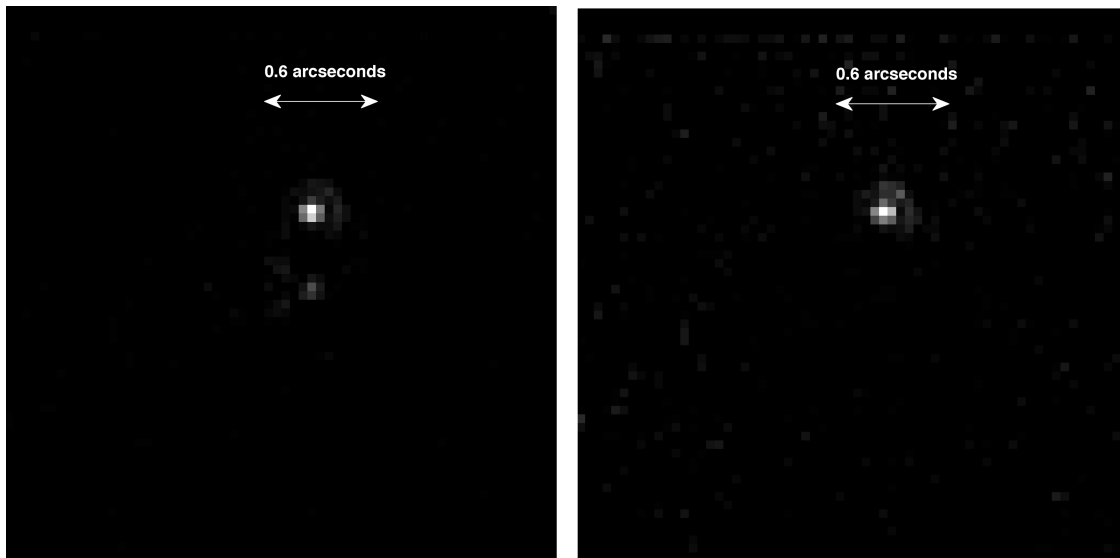


FIG. 1.—The binary image minus the scaled PSF (left) and the subsequent prewhitened binary image (right).

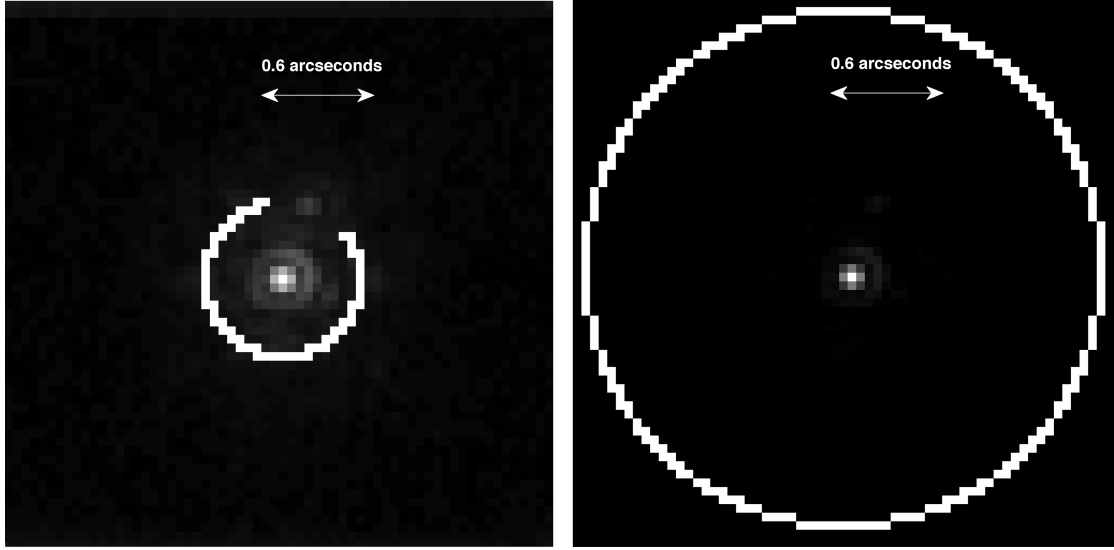


FIG. 2.—SAA image of the binary system HD 170648 (*left*). The white circle denotes the location of the pixels used to estimate the PSNR. The larger circle (*right*) is used to estimate the background.

simple least-squares algorithm; the background, b , was estimated as the mean of an annulus centred at the bright star (see Fig. 2, *right*); and the variance of the detector readout plus background was taken as the variance of the annulus pixel values. The PSNR was computed in the following way (Gladysz & Christou 2008): the peak pixel value from the faint companion was compared to the standard deviation of the noisy pixels

located the same distance away from the bright central star as the companion. This is illustrated in Figure 2 (*left*). The PSNR is given by:

$$\text{PSNR} = \frac{I_{\text{Peak}} - \bar{I}_{\text{ring}}}{\sigma(I_{\text{ring}})}. \quad (27)$$

The PSNR was higher for the prewhitened data (PSNR = 94.2) than for the PSF-subtracted data (PSNR = 65.8) (see Fig. 3).

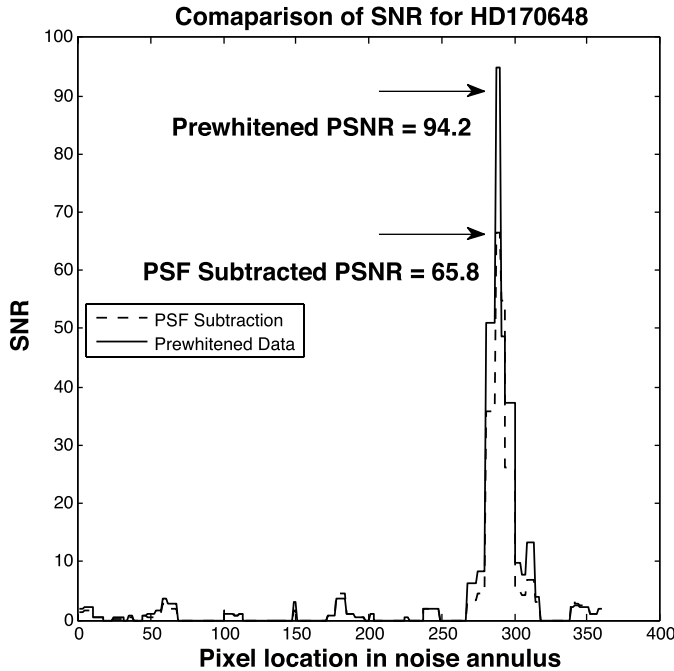


FIG. 3.—Pixel SNR in an annulus around the central star including the companion location.

5. COMPARISON OF TECHNIQUES

In our experiments we tested the accuracy of the photometry and astrometry on relatively low (SR \approx 30%), moderate (SR \approx 40%), and high (SR \approx 50%) data. All three algorithms required an initial estimate of the PSF. This estimate was provided in the form of a calibration PSF observed 10–20 minutes after the science observations. We tested the algorithms with properly matched PSFs ($\Delta\text{SR} = 0.02\%$) and mismatched PSFs ($\Delta\text{SR} = 0.06\%$).

We used observations of four different stars to create these test data: IRAS 21549 + 3929 ($m_V = 12.1$, $m_K = 5.96$), HD 18009 ($m_V = 8.23$, $m_K = 5.02$), HD153832 ($m_V = 7.25$, $m_K = 4.78$), and HD 143209 ($m_V = 6.3$, $m_K = 3.92$). Table 1 shows the PSFs used to create the three data sets.

Artificial binaries ($\Delta m_K = 3.5$ or 4.5 , separation $\theta = 0.6''$) were simulated by scaling and shifting the single-star SAA images. For each case, eight positions for the companion were tested in order to minimize the bias from anisotropy in the PSF (Fig. 4). The mean absolute astrometric and photometric errors were computed based on the results from these eight positions. While the Fitstars algorithm requires an initial estimate of the

TABLE 1
PSFs USED TO SIMULATE BINARY IMAGES

	Science PSF	Reference PSF
Low Strehl		
Matched	IRAS 21549 + 3929 (SR = 0.29)	IRAS 21549 + 3929 (SR = 0.32)
Mismatched	IRAS 21549 + 3929 (SR = 0.29)	HD18009 (SR = 0.35)
Medium Strehl		
Matched	HD15382 (SR = 0.43)	HD15382 (SR = 0.42)
Mismatched	HD15382 (SR = 0.49)	HD15382 (SR = 0.42)
High Strehl		
Matched	HD143209 (SR = 0.54)	HD143209 (SR = 0.52)
Mismatched	HD143209 (SR = 0.54)	HD15382 (SR = 0.49)

PSF, the estimate does not have to be very good, e.g., a single-star image from a different observation run can be used. For these observations, Fitstars was tested with both properly matched and mismatched calibration PSFs. In addition to the PSF estimate, Fitstars also requires an estimate of the initial locations of the stars in the image. These were obtained by visually examining the image. Fitstars was then able to iteratively derive a solution for each star.

The StarFinder PSF-fitting algorithm was designed for the analysis of crowded fields imaged with AO, and the fitting algorithm can take advantage of many estimates of the PSF within the field of view. In our work we provide StarFinder with the PSF estimate—an image of a single star. StarFinder had to be given an estimate for the position of the companion, and we observed that these estimates had to be precise; otherwise the algorithm converged on the brightest static speckle. This situation was treated as nonconvergence.

In the Hotelling approach to estimating differential astrometry (eq. [18]) and photometry (eq. [22]), \bar{g}_0 was modeled as a

scaled version of the reference PSF, the normalized PSF was used for $h(r)$, and finally the covariance matrix of the data was modeled as described in § 4. The location-estimation task was carried out in the following manner; recall that the maximum value of the SSHE (eq. [18]) depends only on the x and y position of the companion, assuming the companion's intensity is known. The Matlab minimization function *fminunc* was used to find the maximum SSHE value. For an initial estimate of the position of the companion in the image, r_0 , the intensity of the companion, A_{pl} , is estimated at r_0 using the OHE (eq. [22]); the SSHE is then computed with the values of $(r_0, A_{pl}(r_0))$. The maximum value is then deemed to be reached when the change in position is less than 0.02 pixels. Once the maximum of the SSHE is found, the values of the companion's position and intensity corresponding to this maximum value are taken as the estimates of these values.

A graphical representation of the values of the SSHE in the region around the location of the companion are presented in

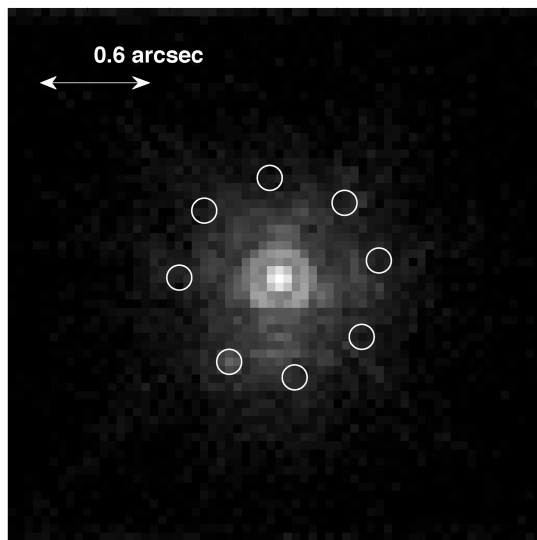


FIG. 4.—The eight artificial companion locations on a circle of radius $0.6''$.

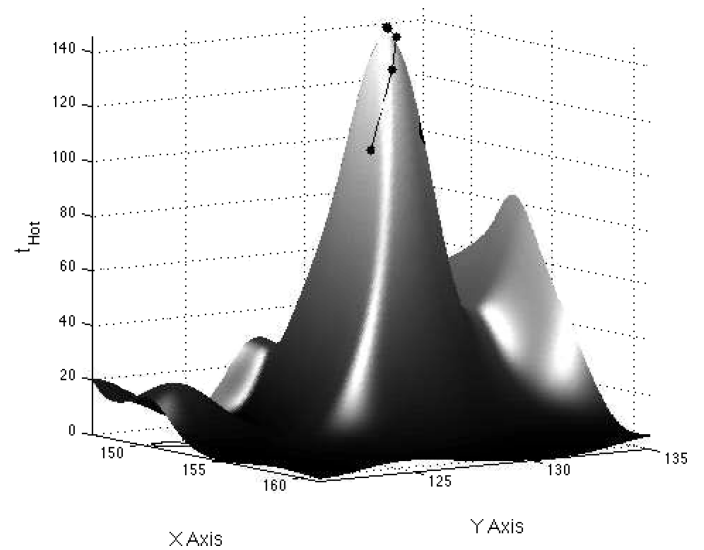


FIG. 5.—The value of the SSHE in the region around the location of the companion; lines and dots show the maximization test points ($\Delta m = 4.5$, $r_{pl} = 0.6''$).

TABLE 2
COMPARATIVE ASTROMETRY ESTIMATION TASK

Δm	PSF Match (SR)	Mean astrometric error		
		(mas)		
		SSHE	Starfinder	Fitstars
High Strehl ($\approx 50\%$)				
3.5	0.2%	0.28	3.0	0.01 (7 failures)
	0.6%	0.37	6.0	3.44 (2 failures)
4.5	0.2%	0.34	3.8	2.65
	0.6%	0.58	11.6	5.67 (5 failures)
Medium Strehl ($\approx 40\%$)				
3.5	0.1%	0.37	7.6	5.97 (4 failures)
	0.7%	0.37	4.5	3.45 (1 failure)
4.5	0.1%	0.65	15.9 (1 failure)	1.96 (3 failures)
	0.7%	0.63	12.8	6.11 (7 failures)
Low Strehl ($\approx 30\%$)				
3.5	0.3%	1.48	24.2	3.09 (5 failures)
	0.6%	1.1	9.8 (5 failures)	4.21 (4 failures)
4.5	0.3%	2.14 (2 failures)	63.5 (5 failures)	2.15 (3 failures)
	0.6%	1.76 (4 failures)	9.1 (7 failures)	3.95 (4 failures)

NOTE.—Failures refer to number nonconvergences of the algorithm for the eight tested locations.

Figure 5. The maximization of the SSHE using this technique reduces the number of test locations, R , such that the computation time for an image from the Lick data is typically less than a second. This execution time is similar to PSF fitting with StarFinder.

5.1. Simulation Results

Tables 2 and 3 present the results for the mean absolute error in astrometry and photometry calculated using the three algo-

rithms on the simulated data. The photometric and astrometric accuracy of the three observers, for the case of a faint companion with a matched PSF, is shown in Figure 6. The Hotelling algorithm always obtained the most accurate estimate for the position of the companion. In all tests, bar one, the Hotelling algorithm returned the most accurate estimate for the relative intensity of the companion. The Hotelling approach performed best on the high SR data set when using a properly matched calibration PSF, and the error in the results increase with decreasing SR.

TABLE 3
COMPARATIVE PHOTOMETRY ESTIMATION TASK

Δm	PSF Match (SR)	Mean $ \Delta \tilde{m} - \Delta m $		
		OHE	Starfinder	Fitstars
High Strehl ($\approx 50\%$)				
3.5	0.2%	0.04	0.05	3.42 (7 failures)
	0.6%	0.03	0.22	0.2 (2 failures)
4.5	0.2%	0.04	0.13	0.84 (1 failure)
	0.6%	0.08	0.43 (4 failures)	0.31 (5 failures)
Medium Strehl ($\approx 40\%$)				
3.5	0.1%	0.05	0.14	1.17 (4 failures)
	0.7%	0.02	0.22	0.48 (1 failure)
4.5	0.1%	0.09	0.32	0.77 (3 failures)
	0.7%	0.1	0.52	0.36 (7 failures)
Low Strehl ($\approx 30\%$)				
3.5	0.3%	0.09	0.46	1.27 (5 failures)
	0.6%	0.12 (2 failures)	0.32	0.125 (4 failures)
4.5	0.3%	0.18 (2 failures)	0.98 (5 failures)	1.21 (4 failures)
	0.6%	0.51 (4 failures)	0.37 (7 failures)	0.34 (4 failures)

NOTE.—Failures refer to number nonconvergences of the algorithm for the eight tested locations.

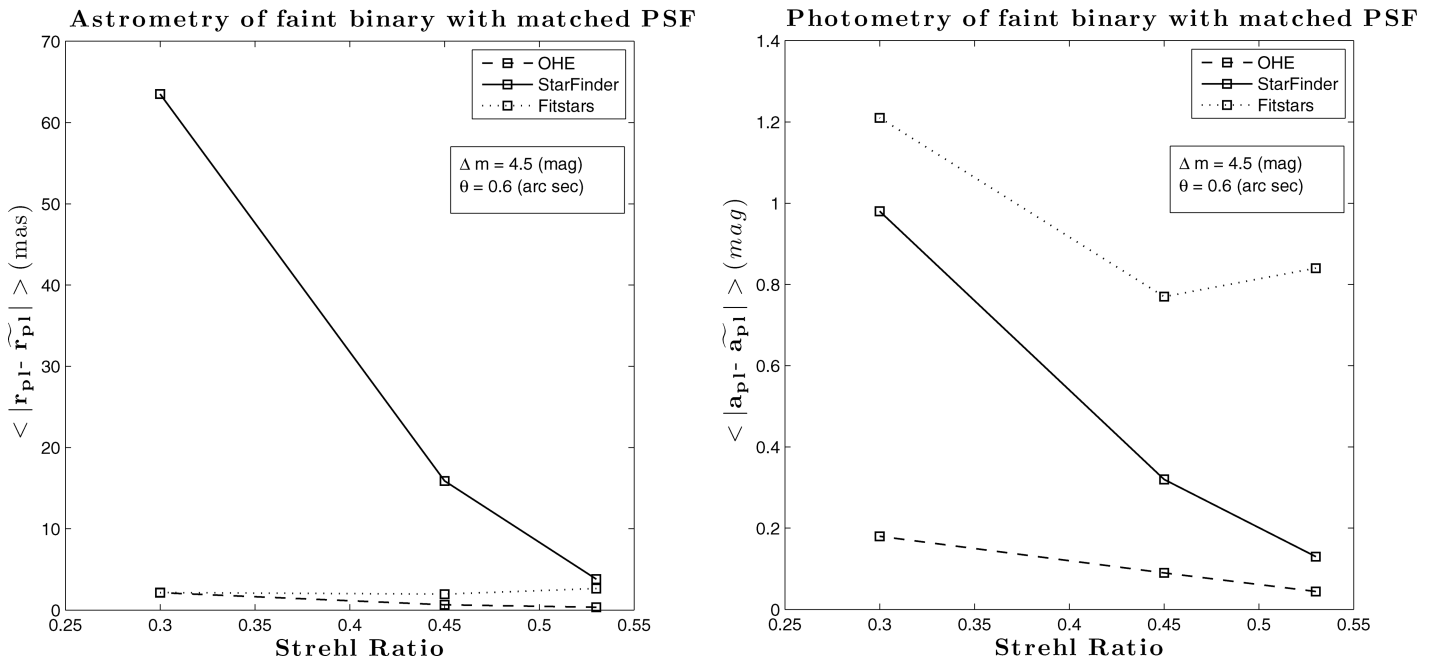


FIG. 6.—Error in astrometry for the three observers (*left*); error in photometry of the faint companion with a matched PSF (*right*). One pixel = 0.76 mas.

As shown in Figure 6, the StarFinder error in astrometry is seen to depend very strongly on the Strehl ratio, with much weaker dependence in the case of Fitstars and the Hotelling observer. However, Fitstars fails to converge more often than the Hotelling algorithm or StarFinder. It is interesting that while StarFinder tends to provide less accurate astrometry than Fitstars, its photometric performance is better.

The ability of Fitstars to handle poor initial estimates of the PSF is shown in the results, where the accuracy using the mismatched PSF is practically the same as when using the matched PSF. This ability also causes the algorithm to perform poorly when the two stars are not well separated. When estimating the PSF, the estimate gets truncated at the midpoint between the two stars. In this data set the two stars are quite close together, $0.6'' \approx 4 \times \text{FWHM}$. Therefore a large amount of the PSF structure was not modeled completely, and this leads to a decrease in the accuracy of the algorithm. This can be clearly seen in the photometry (Fig. 6), because any misestimate of the PSF will cause large errors in the photometry. Astrometry only deals with the central point of the PSF, and is more robust to this error. Fitstars has been shown to produce more accurate photometric measurements with more widely spaced binary stars (Roberts et al. 2005).

6. CONCLUSION

We have presented a new likelihood-maximization method, based on the Hotelling observer, to extract differential astrometry and photometry of faint companions in AO-corrected images. This technique requires knowledge of the data covari-

ance matrix. Multiplying the data by the inverse of the covariance matrix is akin to the familiar signal processing operation of prewhitening. We have shown (see Fig. 3) that performing the prewhitening operation on PSF-subtracted data results in an increase in the pixel S/N in the data.

In § 3, the OHE (eq. [22]) and the IBD equation (eq. [26]) were shown to carry out similar operations on the data to extract differential photometry. However, the OHE incorporates the prewhitening step and therefore has an advantage over IBD in that it is operating in an increased S/N regime.

The Hotelling algorithm produced the most accurate estimates of the position and intensity of the companion. The error on the differential astrometry extracted by the Hotelling algorithm was in general comparable to the error produced by Fitstars. The error in differential photometry returned by the Hotelling algorithm was typically half the error returned by the StarFinder algorithm.

While the algorithm developed in this article assumes Gaussian noise and therefore does not take static speckle noise into account, we have found that it provides better results than standard algorithms when applied to “real” data, i.e., simulated binaries using real single-star observations. Knowledge of static speckle statistics would allow the algorithm to be improved by incorporating this information in the data covariance matrix. This would lead to more effective prewhitening and hence more accurate estimation of the binary star parameters. Alternatively, the static speckle can be reduced by different approaches including SDI (Marois et al. 2000), ADI (Marois et al. 2006), or modulation of the pupil shape (Ribak & Gladysz 2008). In all

these cases, the Hotelling approach can be modified to optimize estimation of the faint companion position and brightness.

This research was funded by Science Foundation Ireland Grant No. 07/IN.1/I906. The authors wish to acknowledge the SFI/HEA Irish Centre for High-End Computing (ICHEC)

for the provision of computational facilities and support. A portion of the research in this article was carried out at the Jet Propulsion Laboratory, California Institute of Technology, under a contract with the National Aeronautics and Space Administration.

REFERENCES

- Aime, C., & Soummer, R. 2004, *ApJ*, 612, L85
- Artigau, E., Biller, B. A., Wahhaj, Z., Hartung, M., Close, L. M., Chun, M. R., Liu, M. C. G. T., Rigaut, F., et al. 2008, in *Proc. SPIE, Ground-based and Airborne Instrumentation for Astronomy II*, ed. I. S. McLean, & M. M. Casali, 7014, 70141Z
- Ayers, G. R., & Dainty, J. C. 1988, *Opt. Lett.*, 13, 547
- Baraffe, I., Chabrier, G., Barman, T. S., Allard, F., & Hauschildt, P. H. 2003, *A&A*, 402, 701
- Barnaby, D., Spillar, E., Christou, J. C., & Drummond, J. D. 2000, *AJ*, 119, 378
- Barrett, H. H., Denny, J. L., Wagner, R. F., & Myers, K. J. 1995, *J. Opt. Soc. Am. A*, 12, 834
- Barrett, H. H., Myers, K. J., Devaney, M. N., & Dainty, J. C. 2006a, *J. Opt. Soc. Am. A*, 23, 3080
- Barrett, H. H., Myers, K. J., Devaney, N., Dainty, J. C., & Caucci, L. 2006b, *Proc. SPIE*, 62721W
- Barrett, H. H., & Myres, K. 2004, *Foundations of Image Science (Weily Series in Pure and Applied Optics)*
- Bauman, B. J., Gavel, D. T., Waltjen, K. E., Freeze, G. J., Keahi, K. A., Kuklo, T. C., Lopes, S. K., Newman, M. J., et al. 1999, *Proc. SPIE*, 3762, 194
- Bloemhof, E. E., Dekany, R. G., Troy, M., & Oppenheimer, B. R. 2001, *ApJ*, 558, L71
- Cagigal, M. P., & Canales, V. F. 1998, *Opt. Lett.*, 23, 1072
- Caucci, L., Barrett, H. H., Devaney, N., & Rodríguez, J. J. 2007, *J. Opt. Soc. Am. A*, 24, B13
- Davis, L. E. 1989, *A User's Guide to the IRAF Apphot Package*
- Devaney, M. N. 1992, *A&A*, 257, 835
- Diolaiti, E., Bendinelli, O., Bonaccini, D., Close, L., Currie, D., & Parmeggiani, G. 2000, *A&AS*, 147, 335
- Fitzgerald, M. P., & Graham, J. R. 2006, *ApJ*, 637, 541
- Fletcher, R. 1987, *Practical Methods of Optimization* (New York: Wiley)
- Gladysz, S., & Christou, J. C. 2008, *ApJ*, 684, 1486
- Gladysz, S., Christou, J. C. 2008, in *ApJ*, 684, 1486
- Gladysz, S., Christou, J. C., & Redfern, M. 2006, *Proc. SPIE*, 6272, I, 62720J
- Helstrom, C. W. 1968, *Statistical Theory of Signal Detection* (Elmsford, NY: Pergamon)
- Horch, E., Ninkov, Z., & Franz, O. G. 2001, *AJ*, 121, 1583
- Jefferies, S. M., & Christou, J. C. 1993, *ApJ*, 415, 862
- Kasper, M. E., Beuzit, J.-L., Verinaud, C., Yaitskova, N., Baudoz, P., Boccaletti, A., Gratton, R. G., Hubin, N., et al. 2008, *Proc. SPIE*, 7015, 70151S
- Lane, R. G. 1992, *J. Opt. Soc. Am. A*, 9, 1508
- Marois, C., Doyon, R., Racine, R., & Nadeau, D. 2000, *PASP*, 112, 91
- Marois, C., Lafrenère, D., Doyon, R., Macintosh, B., & Nadeau, D. 2006, *ApJ*, 641, 556
- Pluzhnik, E. A. 2005, *A&A*, 431, 587
- Press, W. H., Teukolsky, S. A., Vetterling, W. T., & Flannery, B. P. 1986, *Numerical Recipes—The Art of Scientific Computing* (Cambridge: Cambridge Univ. Press)
- Ribak, E. N., & Gladysz, S. 2008, *Optics Express*, 16, 15553
- Roberts, L. C., Jr., Turner, N. H., Bradford, L. W., ten Brummelaar, T. A., Oppenheimer, B. R., Kuhn, J. R., Whitman, K., Perrin, M. D., & Graham, J. R. 2005, *AJ*, 130, 2262
- Roberts, L. C., Jr., Turner, N. H., & ten Brummelaar, T. A. 2007, *AJ*, 133, 545
- Roggemann, M. 1996, *Imaging Through Turbulence* (Boca Raton: CRC Press)
- Shames, P., & Tody, D. 1986, *A User's Introduction to the IRAF Command Language*
- Stetson, P. B. 1987, *PASP*, 99, 191
- . 1992, in *ASP Conf. Ser. 25, Astronomical Data Analysis Software and Systems I*, ed. D. M. Worrall, C. Biemesderfer, & J. Barnes, 297
- Stetson, P. B., Davis, L. E., & Crabtree, D. R. 1990, in *ASP Conf. Ser. 8, CCDs in Astronomy*, ed. G. H. Jacoby, 289
- Stockham, T. G., Cannon, T. M., & Ingebretsen, R. B. 1975, *Proc. IEEE*, 63, 678
- ten Brummelaar, T. A., Mason, B. D., Bagnuolo, W. G., Jr., Hartkopf, W. I., McAlister, H. A., & Turner, N. H. 1996, *AJ*, 112, 1180
- ten Brummelaar, T., Mason, B. D., McAlister, H. A., Roberts, L. C., Jr., Turner, N. H., Hartkopf, W. I., & Bagnuolo, W. G., Jr. 2000, *AJ*, 119, 2403
- Turner, N. H., ten Brummelaar, T., Roberts, L. C., Mason, B. D., Hartkopf, W. I., & Gies, D. R. 2008, *AJ*, 136, 554
- Vasisht, G., Crossfield, I. J., Dumont, P. J., Levine, B. M., Troy, M., Shao, M., Shelton, J. C., & Wallace, J. K. 2006, *Proc. SPIE*, 6272, 627253